Comparison of several staggered atomistic-to-continuum concurrent coupling strategies

D. Davydov[a], J-P. Pelteret[a], P. Steinmann[a,*]

[a] *Chair of Applied Mechanics, University of Erlangen-Nuremberg, Egerlandstr. 5, 91058 Erlangen, Germany*

Abstract

In this contribution several staggered schemes used to couple continuum mechanics (CM) and molecular mechanics (MM) are proposed. The described approaches are based on the atomistic-to-continuum correspondence, obtained by spatial averaging in the spirit of Irving and Kirkwood, and Noll. Similarities between this and other concurrent coupling schemes are indicated, thus providing a broad overview of different approaches in the field. The schemes considered here are decomposed into the surface-type (displacement or traction boundary conditions) and the volume-type. The latter restrict the continuum displacement field (and possibly its gradient) in some sense to the atomistic (discrete) displacements using Lagrange multipliers. A large-strain CM formulation incorporating Lagrange multipliers and a strategy to solve the resulting coupled linear system using an iterative solver is presented.

Finally, the described coupling methods are numerically examined using two examples: uniaxial deformation and a plate with a hole relaxed under surface tension. Accuracy and convergence rates of each method are reported. It was found that the displacement (surface) coupling scheme and the Lagrangian (volume) scheme based on either discrete displacements or the H_1 norm derived from continuous displacement fields provide the best performance.

Keywords: Concurrent multiscale methods, Atomic-to-continuum coupling methods, Molecular mechanics; Irving-Kirkwood-Noll procedure, Finite elements, Large strain

*Corresponding author. Tel.: +49 (0)9131 85 28502, Fax: +49 (0)9131 85 28503

Email addresses: denis.davydov@ltm.uni-erlangen.de (D. Davydov), jean-paul.pelteret@ltm.uni-erlangen.de (J-P. Pelteret), paul.steinmann@ltm.uni-erlangen.de (P. Steinmann)

1. Introduction

In recent decades there has been a growth of interest regarding approaches to couple the description of matter at different scales, namely continuum mechanics (CM), molecular mechanics (MM), and quantum mechanics (QM). Some approaches couple the description in a sequential manner, that is to say the output from a fine scale is directly used in a coarse scale. Usually a more challenging approach is to perform concurrent coupling, in which principally different descriptions are used simultaneously for different parts of the domain. Concurrent coupling methods can be categorized by factors [35] such as the continuum model used, the presence or absence of a "handshake" region, coupling boundary conditions and the governing formulation. Often concurrent methods are tailored for use in a particular type of problem, such as dynamic zero-temperature problems at both continuum and atomistic sides [24, 30, 40] or a quasi-static continuum with either zero [22, 45] or finite [46] temperature atomistic simulations. Very rarely are concurrent coupling schemes applied to amorphous materials [42, 51]. Finally, there are methods that bridge continuum and quantum descriptions [1, 8, 33, 58]. For a general overview we refer the reader to [31, 32, 35].

It is important to note that concurrent methods may require an iterative approach to reach the solution; see for example the Bridging Scale Method (BSM) [45]. Alternatively, there are methods that are formulated in a monolithic manner such as the Quasi-Continuum (QC) [36, 49, 52], the Bridging Domain Method (BDM) [56] and the Arlequin method [5, 44], among others.

Many of the coupling methods directly or indirectly postulate a procedure to compute continuum fields from atomistic simulations which are then used to define the total Hamiltonian and/or constraints on primary (displacements or velocity) fields. In many cases these can be considered as specializations of the theoretical link established by Irving and Kirkwood [18], and Noll [38]. For example, in [28, 50] the authors explicitly use results of the atomistic-to-continuum correspondence in conjunction with the delta-function as an averaging kernel to calculate cell-integrated quantities which are then used in the coupling procedure. Monolithic methods which use a handshake interface between atomistic and continuum domains [5, 44, 56] require the localization of the potential energy to a spatial point in order to define the total Hamiltonian for the system.

Although monolithic concurrent coupling schemes such as the QC, BDM or Arlequin methods are, in general, computationally faster than staggered coupling schemes, there are several reasons why utilizing the latter may be desirable. First, if one considers a thermo-mechanical quasi-static problem, there is a clear time-scale separation between the two descriptions. This often leads to a definition of the

temperature field in terms of time-averaged atomistic fluctuations. In such a case there is, it seems, no other choice but to solve the two problems independently while coupling using staggered approaches. This is partly due to the fact that it is the free-energy which is considered in CM. This quantity is not immediately available from MM[1] and thus blending the two to derive a variational formulation is not trivial. As an example, one of the extensions of the QC method to finite temperatures [14] effectively leads to a staggered solution approach. Alternatively, one can construct effective (coarse-grained) thermodynamic potentials based on the principle of maximum entropy. Using this approach coupling at non-uniform temperatures can be achieved in a monolithic manner using, for example, another extension of the QC method [3, 23].

Staggered schemes may be applied not only to couple MM and CM, but also CM and QM [33, 58]. In the latter case, the principal differences between governing equations[2] lead to staggered approaches being widely adopted. Note that the QM Hamiltonian is defined for the system as a whole, as opposed to the MM Hamiltonian which is attributed to collections of, at most, four particles.

The blending of CM and MM Hamiltonians is relatively simple when the systems considered on the MM side consist of two-point potentials. In such a case the energy attributed to each bond is situated at the geometric center of particle pairs and is blended with the CM Hamiltonian according to a chosen weighting function. This, however, becomes much more complicated and less unique for cases when three- and four-point potentials are considered. To the best of our knowledge, coupling methods based on the blending of Hamiltonians have not been applied to such cases. Even for pair-potentials, bonds can be weighted in different ways; see the discussion in [22, 56] and the references therein. The issue is principally similar to that of localizing the potential energy of a particle system in order to obtain the balance of energy in terms of atomistic quantities [12]. One further method to localize the potential energy for the purpose of coupling atomistic and continuum models is proposed in [22].

Finally, staggered schemes are easier to implement in a non-intrusive fashion when utilizing third-party finite-element (FE) and molecular dynamics (MD) codes.

Staggered methods do not need to define the total Hamiltonian in order to derive the governing equations for the system as a whole from a variational principle. Even

[1]There are a few methods that describe how to obtain the free-energy macroscopically, such as the integration of stresses with respect to the applied deformation gradient while keeping the temperature fixed.

[2]The Kohn-Sham equations of the density functional theory on the QM side leads to an general eigenvalue problem as opposed to the partial differential equations on the CM side

though this is the case, constraints between the corresponding kinematic and/or kinetic quantities have to be introduced. In the most simple case, such constraints can be imposed through the exchange of boundary conditions between the MM and CM formulations; see for example [39, 48]. Other staggered approaches will be proposed and considered in the main body of this contribution.

As it is clear from the short review in the above, there is an immense variety of methods that couple different descriptions of matter concurrently. It is difficult to compare approaches since each method is unique in terms of the description of the governing equations, the continuum model and boundary conditions that are used, and whether a handshake region is introduced. We are aware of only one publication [35] in which different coupling methods are compared using the same test cases.

In this contribution, we aim at comparing different coupling approaches based on the atomistic-to-continuum correspondence. We focus on the aspect related to both staggered and monolithic schemes, namely the method used to constrain fields, while keeping the other parts of the coupled formulation the same. We benchmark different approaches of transferring information between the atomistic and continuum domains in the context of staggered schemes. Coupling strategies are studied numerically using two plane-strain examples and the results are compared to a full atomistic simulation.

The rest of the paper is organized as follows: In Section 2 we review the basics of calculating fields from atomistic (discrete) simulations pioneered in the works of Irving and Kirkwood, and Noll. Some general ideas with regards to staggered schemes are presented in Section 3. In section 4 we describe four different coupling strategies (two volume-type and two surface-type) based on the atomistic-to-continuum correspondence. In Section 5 we obtain the weak form for the continuum formulation. Furthermore we discuss the solution strategy for the resulting system of equations, including the preconditioners used in iterative solvers. The proposed staggered strategies are then numerically studied in Section 6 using two problems, namely that of uniaxial deformation of a plate and relaxation of a plate with a hole under surface tension. Convergence rates and error measures are reported. Lastly a discussion and conclusions are presented in Section 7.

2. Atomistic to continuum link

In this section we briefly remind the reader of the atomistic-to-continuum correspondence based on the Irving and Kirkwood [18], and Noll [38] approach. In particular we will limit ourselves to the Lagrangian averaging [10, 59] approach. This idea seemed to be first mentioned in [28, p 1656]. As was shown by the authors

in previous works [9], this approach leads to the same results as Eulerian averaging when applied to the solids studied in this paper. For more details we refer the reader to [10–13, 18, 37, 38, 59] and the references therein.

The discrete displacement of each atom is introduced as

$$\mathsf{u}^\alpha = \mathsf{x}^\alpha - \mathsf{X}^\alpha \tag{1}$$

where x^α is the current position of a particle, and X^α represents its reference position. In the case of molecular statics x^α is determined by minimizing the total (atomistic) potential energy of the system, that is $\min_{\mathsf{x}^\alpha}[\Pi^{\mathrm{a}}_{\mathrm{int}} - \Pi^{\mathrm{a}}_{\mathrm{ext}}]$, and X^α can be taken as the initial position of the atoms. By index a we denote quantities related to atomistic simulations. In contrast, in the molecular dynamic case the latter are statistically averaged positions of atoms in the initial state of the system. For more details regarding the second case see [10]. The inter-particle distance vector is denoted by $\mathsf{X}^{\alpha\beta} = \mathsf{X}^\alpha - \mathsf{X}^\beta$.

Performing averaging in the reference configuration via the spatial (isotropic) kernel $w(\mathsf{X}^\alpha - \boldsymbol{X}) \equiv w(|\mathsf{X}^\alpha - \boldsymbol{X}|)$, expressions for numerous CM fields that satisfy the CM balance equations may be derived. Here $\boldsymbol{X}$ denotes the CM coordinate in the material configuration.

In this way, the referential mass density is defined as

$$\varrho_{\mathrm{a}}(\boldsymbol{X}) := \sum_\alpha \mathsf{m}^\alpha w(\mathsf{X}^\alpha - \boldsymbol{X}), \tag{2}$$

from which the displacement can be obtained as

$$\boldsymbol{u}_{\mathrm{a}}(\boldsymbol{X}) := \frac{\sum_\alpha \mathsf{m}^\alpha \mathsf{u}^\alpha w(\mathsf{X}^\alpha - \boldsymbol{X})}{\sum_\alpha \mathsf{m}^\alpha w(\mathsf{X}^\alpha - \boldsymbol{X})}, \tag{3}$$

with the corresponding deformation gradient given by

$$\boldsymbol{F}_{\mathrm{a}}(\boldsymbol{X}) = \boldsymbol{I} + \frac{\sum_\alpha \mathsf{m}^\alpha [\mathsf{u}^\alpha - \boldsymbol{u}(\boldsymbol{X})] \otimes \mathrm{Grad} w(\mathsf{X}^\alpha - \boldsymbol{X})}{\varrho_{\mathrm{a}}(\boldsymbol{X})}. \tag{4}$$

Furthermore, the Piola stress is obtained as

$$\boldsymbol{P}_{\mathrm{a}}(\boldsymbol{X}) = -\frac{1}{2}\sum_\alpha \mathsf{f}^{\alpha\beta} \otimes \mathsf{X}^{\alpha\beta} \widehat{w}^{\alpha\beta} \tag{5}$$

with

$$\widehat{w}^{\alpha\beta}(\boldsymbol{X}, \mathsf{X}^\alpha, \mathsf{X}^\beta) = \int_0^1 w\big(\mathsf{X}^\alpha - \boldsymbol{X} - a\mathsf{X}^{\alpha\beta}\big)\, \mathrm{d}a \tag{6}$$

where $\mathbf{f}^{\alpha\beta}$ is the force exerted on atom α by atom β.

Note that the averaging (smoothing) operation (in particular Eq. (3)) can be considered as a specialized case of the projection from the space of discrete displacements defined at the reference positions $\mathbf{X}^{\alpha}$ to a continuum function defined at an arbitrary point $\boldsymbol{X}$ in the reference configuration.

3. Staggered coupling schemes

The main feature of staggered coupling schemes is that the solution to the coupled problem is obtained iteratively by solving the corresponding atomistic and continuum parts sequentially. Generally, the domain of interest $\Omega = \Omega_{\mathrm{c}} \cup \Omega_{\mathrm{a}}$ is split into two domains Ω_{a} and Ω_{c} respectively to which the atomistic and continuum descriptions are applied. This decomposition is highlighted in Fig. 1(a). Depending on the coupling approach, these domains could have either zero or non-zero intersection. Below we will consider staggered coupling strategies with non-zero intersection, that is for which $\Omega_{\mathrm{c}} \cap \Omega_{\mathrm{a}} =: \Omega_{\mathrm{a+c}} \neq \emptyset$. A staggered scheme of coupling leads explicitly or implicitly to the transfer of "information" between the two approaches. This can be achieved by introducing two additional non-intersecting regions $\Omega_{\mathrm{p}} \subset \Omega_{\mathrm{a+c}}$ and $\Omega_{\mathrm{HS}} \subset \Omega_{\mathrm{a+c}}$ which are also shown in Fig. 1(a). In the former region the information is passed from the continuum description to the atomistic one (C2A), whereas in the latter the transfer occurs in the opposite direction (A2C).

For the case of molecular dynamics, other regions might be used to control the temperature in the atomistic domain and/or to transfer heat fluxes to the continuum description, such as is done in [46]. It is also possible to apply displacement and temperature boundary conditions in the same region simultaneously. This was achieved in [28] by dividing fields into a mean part (which is given by the continuum solution) and a fluctuating part on which the Nose Hoover thermostat was applied.

Since we restrict the current study to molecular statics, we will not discuss issues related to passing temperature (or heat flux) between the different formulations.

3.1. Continuum-to-Atomistic direction

To make the study more focused, we use an affine assumption for the displacements of atoms in Ω_{p} (called padding atoms) to perform C2A transfer. Atoms in this region are fully enslaved to the continuum solution and are displaced according to the continuum fields. This strong-coupling approach is used in many coupling schemes [15, 39, 45, 46, 53, 54]. This type of coupling can also be considered as a special case of the BDM [56] and the Arlequin [5, 44] approach if, instead of a smooth function to blend the continuum and the atomistic Hamiltonians, a Heaviside function is employed. As a result, those atoms whose energy does not contribute to the

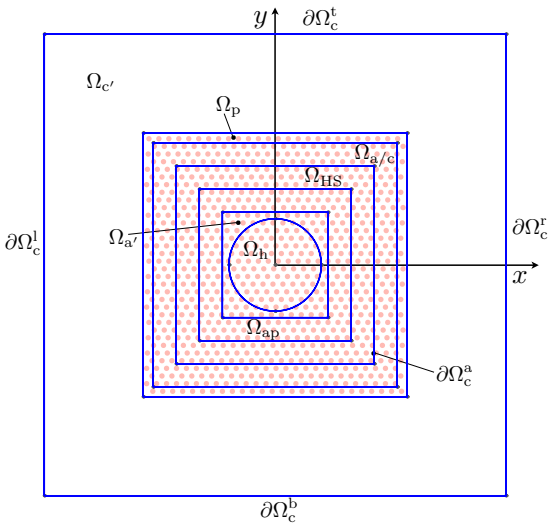

(a) Domains considered in staggered scheme

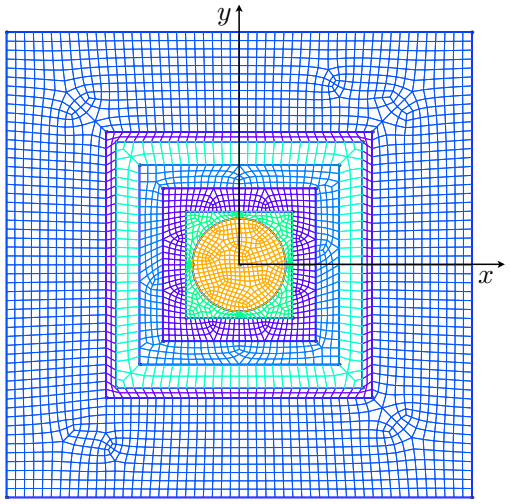

(b) Union of the continuum and atomistic meshes

Figure 1: The domains and the corresponding mesh considered in the staggered coupling methods; (a): The following domains are illustrated: the pure atomistic domain $\Omega_{a'}$, the domain from which atoms will be removed to produce a cavity Ω_h, the handshaking region Ω_{HS}, the domain with padding atoms Ω_p. Two auxiliary domains ($\Omega_{a/c}$ and Ω_{ap}) are introduced to speed up the calculation of fields in Ω_{HS} by considering only such atoms α with $\mathbf{X}^\alpha \in \{\Omega_{HS} \cup \Omega_{a/c} \cup \Omega_{ap}\}$. The size of these domains were chosen to be large enough compared to the averaging radius and the maximum pair interaction cut-off radius. As a result, the total atomistic and continuum domains are given by $\Omega_a = \Omega_h \cup \Omega_{a'} \cup \Omega_{ap} \cup \Omega_{HS} \cup \Omega_{a/c} \cup \Omega_p$ and $\Omega_c = \Omega_{c'} \cup \Omega_p \cup \Omega_{a/c} \cup \Omega_{HS}$ respectively. The boundary of the continuum domain is $\partial\Omega_c = \partial\Omega_c^a \cup \partial\Omega_c^l \cup \partial\Omega_c^r \cup \partial\Omega_c^b \cup \partial\Omega_c^t$; (b): The union of the corresponding meshes used for both the continuum formulation and the calculation of fields from atomistic simulations.

total Hamiltonian of the system will move solely in such a way as to minimize the difference measure between the continuum displacements and atomistic (discrete) displacements. This will result in atomistic displacements similar, if not equivalent, to the affine displacement approach used here.

In the interest of brevity, we do not delve deeper into this discussion. However we consider it important to indicate similarities between different coupling approaches. The general problem of applying boundary conditions to the atomistic description

has been studied in [20, 21, 26, 27, 29].

3.2. Atomistic-to-Continuum direction

The transfer of information in the opposite direction will be based on the fundamental link between the atomistic and continuum description of matter described in Section 2. Let us note that this is not the only conceivable approach that may be used to relate MM to CM quantities and, in particular, to calculate the displacement field based on the atomistic solution. Other approaches include, but are not limited to: displacement decomposition into coarse and fine scales [22, 24, 40, 45, 47, 55], Lagrange interpolation polynomial [39], linear interpolation [6, 41, 44], moving least-square approximation [57]. Most of these coupling methods explicitly or implicitly use a link between some of the discrete quantities and their continuum counterparts.

In the next sections we describe a number of different possible coupling strategies based on the atomistic-to-continuum correspondence considered here, as well as indicate their similarities to other approaches available in the literature.

4. Coupling strategies

4.1. Surface-type

We propose two surface-type coupling methods in which information is passed from the atomistic simulation to the continuum domain on the boundary $\partial\Omega_{\mathrm{c}}^{\mathrm{a}}$ by applying either Dirichlet or Neumann boundary conditions.

4.1.1. Kinematics

A number of methods have been developed to use the results of atomistic simulations to provide displacement boundary conditions to the continuum domain; see for example [46, 48]. Although in [48] the authors did not specifically discuss the theoretical link between the atomistic and continuum descriptions, their approach that evaluates the displacement of the center of mass of atoms in Voronoi-type cells attributed to each FE node can be considered as a particular case of Eq. (3)[3]. More precisely $w = 1/V_{\mathrm{voronoi}}$ in each Voronoi cell and $w = 0$ elsewhere. For such a case Eq. (3) gives the displacement of the center of mass.

Many methods that require refinement of the mesh to an atomistic level can also be attributed to this group since they constrain the displacement of a given node

[3] In [48] the authors consider molecular dynamics and therefore utilize additional time averaging. In our approach this will only add additional probability averaging (which is replaced with time averaging using an Ergodic assumption). This was demonstrated in [10]. Similarities between the two coupling approaches still hold true.

to the displacement of a particle with a reference coordinate that coincides with the referential FE node. This result follows from postulating the atomistic displacement fields using the Dirac delta distribution function δ

$$\boldsymbol{u}_{\mathrm{a}}(\boldsymbol{X},\tau) := \frac{\sum_{\alpha} \mathsf{m}^{\alpha}\mathbf{u}^{\alpha}\delta(\mathbf{X}^{\alpha}-\boldsymbol{X})}{\sum_{\alpha} \mathsf{m}^{\alpha}\delta(\mathbf{X}^{\alpha}-\boldsymbol{X})}, \tag{7}$$

which leads to the following displacement boundary condition as evaluated at each node

$$\boldsymbol{u}_{\mathrm{a}}(\boldsymbol{X}_I,\tau) = \mathbf{u}^{\alpha}, \;\; \exists\alpha : \mathbf{X}^{\alpha} \equiv \boldsymbol{X}_I. \tag{8}$$

As a possible coupling strategy we impose displacement boundary conditions on $\partial\Omega_{\mathrm{c}}^{\mathrm{a}}$ as evaluated using Eq. (3) from the atomistic simulations.

4.1.2. Kinetics

Coupling at the level of fluxes is performed in the heterogeneous multiscale method [28, 30]. These authors employed the finite volume method to solve the continuum equations, and therefore required that the integral of the flux (stress) over the cell had to be calculated from atomistic simulations. This was achieved by employing the results of Section 2 in conjunction with the Dirac δ-distribution as an averaging kernel.

As an alternative coupling approach, we propose that the referential traction boundary conditions associated with the continuum domain are given by

$$\boldsymbol{T}_{\mathrm{a}}(\boldsymbol{X}) = \boldsymbol{P}_{\mathrm{a}}(\boldsymbol{X}) \cdot \boldsymbol{N}(\boldsymbol{X}) \tag{9}$$

where $\boldsymbol{P}_{\mathrm{a}}(\boldsymbol{X})$ is the Piola stress calculated from the atomistic simulation via Eq. (5) and $\boldsymbol{N}$ is the outer normal to the boundary $\partial\Omega_{\mathrm{c}}^{\mathrm{a}}$.

4.2. Volume-type

4.2.1. Discrete displacements

Many coupling schemes introduce constraints between continuum and atomistic degrees-of-freedom in a certain region where both descriptions coexist [2, 15, 25, 34]. This region is usually called a handshaking region and is denoted here by Ω_{HS}. Lagrange multipliers or augmented Lagrange multipliers [7] are normally used to impose such constraints.

One possible approach, such as that presented in [2][4], is to introduce constraints for each atom in the handshaking region in a strong form, namely

$$\mathbf{g}^{\alpha} = \boldsymbol{u}(\mathbf{X}^{\alpha}) - \mathbf{u}^{\alpha} = \mathbf{o} \quad \forall\alpha : \mathbf{X}^{\alpha} \in \Omega_{\mathrm{HS}}. \tag{10}$$

[4]Note that although in this work the authors constrained velocities, this does not affect the discussion about different possibilities that may be used to impose constraints.

The above requirement can be written in its continuum form as

$$\Delta \boldsymbol{u}(\boldsymbol{X}) := \sum_{\alpha} [\boldsymbol{u}(\mathbf{X}^{\alpha}) - \mathbf{u}^{\alpha}] \delta(\boldsymbol{X} - \mathbf{X}^{\alpha}) = \mathbf{o} \quad \forall \boldsymbol{x} \in \Omega_{\mathrm{HS}}, \tag{11}$$

which was used in [15].

Note that this is nothing other than the postulation of the continuum field of displacement mismatch $\Delta \boldsymbol{u}(\boldsymbol{X})$ as opposed to defining the atomistic displacement field $\boldsymbol{u}_{\mathrm{a}}$ itself (through Eq. (3) or Eq. (7)). Differing from the Irving-Kirkwood and Noll approach, this definition can not be used to obtain the corresponding flux quantities for the CM balance laws.

Alternatively [15, 25, 34], the continuity of displacements can be imposed in a weak sense, that is by minimizing the (weighted) least square difference between continuum and discrete atomistic displacements:

$$g = \sum_{\alpha} [\boldsymbol{u}(\mathbf{X}^{\alpha}) - \mathbf{u}^{\alpha}]^2 \tag{12}$$

or

$$g = \sum_{\alpha} \mathsf{m}^{\alpha} [\boldsymbol{u}(\mathbf{X}^{\alpha}) - \mathbf{u}^{\alpha}]^2. \tag{13}$$

The mass-weighted case was used in the BSM [55] to define the projection operator that relates atomistic displacements to their continuum counterparts. The continuum version of such constraints are used in the BDM [56] and in the coupling stress-force method [15] in the form of the constraint

$$g = \int_{\Omega_{\mathrm{HS}}} \Delta \boldsymbol{u}(\boldsymbol{x}) \cdot \Delta \boldsymbol{u}(\boldsymbol{x}) \, \mathrm{d}V = \int_{\Omega_{\mathrm{HS}}} \sum_{\alpha} [\boldsymbol{u}(\mathbf{X}^{\alpha}) - \mathbf{u}^{\alpha}]^2 \delta(\boldsymbol{x} - \mathbf{x}^{\alpha}) \, \mathrm{d}V. \tag{14}$$

For the current study, we will consider constraints as given in Eq. (14) imposed on the continuum formulation by continuous Lagrange multipliers. Details of the formulation and corresponding weak forms will be presented later.

4.2.2. Averaged displacements

In the previous section, the difference between the continuum displacement field and the discrete displacements was introduced in a point-wise manner. Alternatively, one can first define a projection operator which can be used to obtain a field based on the atomistic displacements. In this contribution, this is achieved through the use of Eq. (3). Given the smoothed atomistic displacement field, the compatibility between the atomistic and continuum domains can be enforced both in terms of

the displacement field and its gradient (H_1 norm). Such constraints, as used in the Arlequin[5] coupling method [5, 41, 44], in the most general case read as

$$g = |\boldsymbol{u} - \boldsymbol{u}_{\mathrm{a}}| = \int_{\Omega_{\mathrm{HS}}} \beta_1 [\boldsymbol{u} - \boldsymbol{u}_{\mathrm{a}}] \cdot [\boldsymbol{u} - \boldsymbol{u}_{\mathrm{a}}] + \beta_2 [\mathrm{Grad}\boldsymbol{u} - \mathrm{Grad}\boldsymbol{u}_{\mathrm{a}}] : [\mathrm{Grad}\boldsymbol{u} - \mathrm{Grad}\boldsymbol{u}_{\mathrm{a}}] \, \mathrm{d}V \tag{15}$$

where β_1 and β_2 are non-negative weight parameters. The case of $\beta_1 = 1$ and $\beta_2 = 0$ is equivalent to the L_2 norm on Ω_{HS}, $\beta_1 = 0$ and $\beta_2 = 1$ gives the H_1 seminorm, and finally $\beta_1 = 1$ and $\beta_2 = 1$ corresponds to the H_1 norm. Note, that $\| \cdot \|_{L_2} \leqslant \| \cdot \|_{H_1}$.

The main difference between this approach and the discrete displacement coupling constraints presented previously is that the atomistic displacement field, as opposed to the displacement difference, is introduced in the H_1 error norm. From this follows the need to calculate the gradient of the displacement, which is, obviously, not available as a discrete quantity attributed to each particle. Thus the discrete displacement $\mathbf{u}^{\alpha}$ first needs to be projected onto a space of continuous functions and only then the error norm can be used. In such a case, constraints are available only in the weak form, as opposed to that given in Eq. (10).

Often Arlequin coupling constraints (Eq. (15)) are imposed using a continuous Lagrange multipliers field $\boldsymbol{\lambda}(\boldsymbol{X})$ as

$$g_{\lambda} = \int_{\Omega_{\mathrm{HS}}} \beta_1 \boldsymbol{\lambda} \cdot [\boldsymbol{u} - \boldsymbol{u}_{\mathrm{a}}] + \beta_2 \mathrm{Grad}\boldsymbol{\lambda} : [\mathrm{Grad}\boldsymbol{u} - \mathrm{Grad}\boldsymbol{u}_{\mathrm{a}}] \, \mathrm{d}V. \tag{16}$$

Note that the original formulation of the Areqluin coupling method requires the definition of a global Hamiltonian which is postulated as a mixture of Hamiltonians attributed to each type of domains (atomistic and continuum). As a result, this allows for the formulation of a monolithic coupled problem for which the solution is obtained from a single system of linearized equations. One way to translate this to a staggered scheme is to divide it into two blocks. The first block represents continuum displacements and Lagrange multipliers and the second the atomistic displacements. Subsystems related to those two blocks can then be solved iteratively. Due to this, the continuum displacements and Lagrange multipliers are decoupled from the atomistic displacements. This staggered scheme was used in [57] and in [41] (named "Type Ia").

In this paper, however, we will study the Arlequin-type constraints (Eq. (15)) without blending of the Hamiltonians since we aim at investigating performance

[5] In general this is not a staggered method, i.e. the solution to the coupled system is obtained in one step by solving the resulting system of linear equations.

and efficiency of the different coupling schemes. Another difference between our and previous works lies in the C2A link, for which the general Arlequin formulation follows from the total Hamiltonian. In contrast we impose it by displacing padding atoms according to the continuum solution. This, however, can be considered as a particular case of weighting Hamiltonians, as mentioned in Section 3.1.

5. General formulation of the continuum problem

5.1. Balance equations and linearisation of large-strain formulation

We consider the general case of the continuum balance equations with both Dirichlet and Neumann boundary conditions together with the constraints introduced via Lagrange multipliers. Formulations corresponding to each of the coupling strategies discussed in Section 4 will be obtained as a particular case of the general formulation.

Consider the following non-linear boundary value problem which corresponds to continuum quasi-static equations of motion in the material (Lagrangian) description:

$$\mathrm{Div}\boldsymbol{P} + \boldsymbol{B} = \mathbf{o} \tag{17}$$

$$\boldsymbol{u} = \overline{\boldsymbol{u}} \qquad \text{on } \partial\Omega_{\mathrm{c}}^{\mathrm{u}} \tag{18}$$

$$\boldsymbol{T} = \boldsymbol{P}\cdot\boldsymbol{N} = \overline{\boldsymbol{T}} \qquad \text{on } \partial\Omega_{\mathrm{c}}^{\sigma}, \tag{19}$$

where

$$\partial\Omega_{\mathrm{c}} = \partial\Omega_{\mathrm{c}}^{\mathrm{u}} \cup \partial\Omega_{\mathrm{c}}^{\sigma} \quad \text{with} \quad \partial\Omega_{\mathrm{c}}^{\mathrm{u}} \cap \partial\Omega_{\mathrm{c}}^{\sigma} = \emptyset. \tag{20}$$

Here $\boldsymbol{P}$, $\boldsymbol{B}$, $\overline{\boldsymbol{u}}$, $\overline{\boldsymbol{T}}$ denote the Piola stress, referential body force, prescribed boundary displacement and prescribed Piola traction vector (force per unit reference surface area) respectively.

Multiplying Eq. (17) by a vector-valued test function $\delta\boldsymbol{u}$ which satisfies

$$\delta\boldsymbol{u} = \mathbf{o} \ \text{ on } \ \partial\Omega_{\mathrm{c}}^{\mathrm{u}} \tag{21}$$

and using the divergence theorem, the weak form follows as

$$F(\boldsymbol{u},\delta\boldsymbol{u}) = \int_{\Omega_{\mathrm{c}}} [\boldsymbol{P} : \mathrm{Grad}\delta\boldsymbol{u} - \boldsymbol{B}\cdot\delta\boldsymbol{u}]\,\mathrm{d}V - \int_{\partial\Omega_{\mathrm{c}}^{\sigma}} \overline{\boldsymbol{T}}\cdot\delta\boldsymbol{u}\,\mathrm{d}S = 0. \tag{22}$$

Next, we limit ourselves by considering conservative mechanical systems[6]. There exists a total potential energy functional Π of the system defined as the sum of the internal Π_{int} and external Π_{ext} potential energies

$$\Pi = \Pi_{\text{int}} + \Pi_{\text{ext}} \tag{23}$$

$$\Pi_{\text{int}} = \int_{\Omega_{\text{c}}} \Psi(\boldsymbol{F}(\boldsymbol{u}))\,\mathrm{d}V \tag{24}$$

$$\Pi_{\text{ext}} = -\int_{\Omega_{\text{c}}} \boldsymbol{B}\cdot\boldsymbol{u}\,\mathrm{d}V - \int_{\partial\Omega_{\text{c}}^{\sigma}} \overline{\boldsymbol{T}}\cdot\boldsymbol{u}\,\mathrm{d}S \tag{25}$$

where $\Psi(\boldsymbol{F}(\boldsymbol{u}))$ denotes the strain-energy per unit reference volume.

The principle of stationary potential energy[7] requires that the directional derivative with respect to the displacements $\boldsymbol{u}$

$$\delta\Pi(\boldsymbol{u},\delta\boldsymbol{u}) = D_{\delta\boldsymbol{u}}\Pi(\boldsymbol{u}) = \frac{\mathrm{d}}{\mathrm{d}\epsilon}\Pi(\boldsymbol{u}+\epsilon\,\delta\boldsymbol{u})\bigg|_{\epsilon=0} = 0 \tag{26}$$

vanishes in all directions $\delta\boldsymbol{u}$ at the equilibrium state. The arbitrary vector field $\delta\boldsymbol{u}$ should satisfy Eq. (21). The stationary conditions (Eq. (26)) yields precisely the weak form of quasi-static balance equations (Eq. (22)) with the constitutive equation $\boldsymbol{P} = \partial\Psi/\partial\boldsymbol{F}$. In other words, for systems that allow the introduction of a strain-energy function, the solution to Eq. (22) corresponds to the stationary point of a functional; the total potential energy is stationary if, and only if, Eq. (22) is satisfied.

Based on the stationary potential energy variational principle, we can introduce constraints, namely Eq. (15), to the displacement field. Specifically, this can be achieved by introducing a term with Lagrange multipliers $g_\lambda(\boldsymbol{u},\boldsymbol{\lambda})$ to the total potential energy and solving the saddle point problem

$$\inf_{\boldsymbol{u}}\sup_{\boldsymbol{\lambda}} \Pi^*(\boldsymbol{u},\boldsymbol{\lambda}), \tag{27}$$

where $\Pi^*(\boldsymbol{u},\boldsymbol{\lambda}) = \Pi_{\text{int}}(\boldsymbol{u}) + \Pi_{\text{ext}}(\boldsymbol{u}) + g_\lambda(\boldsymbol{u},\boldsymbol{\lambda})$. On denoting the vector of unknowns

[6]This is a subclass of general systems, which does not include problems such as heat dissipation, propagation of a crack, etc. In other words, Eq. (22) is a more general description which allows non-conservative constitutive models $\boldsymbol{P} = \boldsymbol{P}(\boldsymbol{F};\text{internal variables})$.

[7]Its generalization to dynamics is the Hamilton's variational principle: $\delta\int_{t_0}^{t_1} L(\boldsymbol{u},\dot{\boldsymbol{u}})\,\mathrm{d}t = 0$ where $L(\boldsymbol{u},\dot{\boldsymbol{u}}) = \Pi(\boldsymbol{u}) - K(\dot{\boldsymbol{u}})$ and K denotes kinetic energy. This principle yields the weak form of the dynamic continuum balance equations.

and its variation as

$$\boldsymbol{U} = \left[\begin{array}{c} \boldsymbol{u} \\ \boldsymbol{\lambda} \end{array} \right], \quad \delta\boldsymbol{U} = \left[\begin{array}{c} \delta\boldsymbol{u} \\ \delta\boldsymbol{\lambda} \end{array} \right] \tag{28}$$

the stationary condition $\delta\Pi^*(\boldsymbol{U}, \delta\boldsymbol{U}) = 0$ results in

$$\begin{aligned} \frac{\partial \Pi}{\partial \boldsymbol{u}} \cdot \delta\boldsymbol{u} + \frac{\partial g_\lambda}{\partial \boldsymbol{u}} \cdot \delta\boldsymbol{u} + \frac{\partial g_\lambda}{\partial \boldsymbol{\lambda}} \cdot \delta\boldsymbol{\lambda} = & \int_{\Omega_\mathrm{c}} \boldsymbol{S}(\boldsymbol{E}(\boldsymbol{u})) : \delta\boldsymbol{E}(\boldsymbol{u}, \delta\boldsymbol{u}) \, \mathrm{d}V \\ & - \int_{\Omega_\mathrm{c}} \boldsymbol{B} \cdot \delta\boldsymbol{u} \, \mathrm{d}V - \int_{\partial\Omega_\mathrm{c}^\sigma} \overline{\boldsymbol{T}} \cdot \delta\boldsymbol{u} \, \mathrm{d}S \\ & + \beta_1 \int_{\Omega_\mathrm{HS}} \boldsymbol{\lambda} \cdot \delta\boldsymbol{u} \, \mathrm{d}V + \beta_2 \int_{\Omega_\mathrm{HS}} \mathrm{Grad}\boldsymbol{\lambda} : \mathrm{Grad}\delta\boldsymbol{u} \, \mathrm{d}V \\ + \beta_1 \int_{\Omega_\mathrm{HS}} [\boldsymbol{u} - \boldsymbol{u}_\mathrm{a}] \cdot \delta\boldsymbol{\lambda} \, \mathrm{d}V + \beta_2 & \int_{\Omega_\mathrm{HS}} [\mathrm{Grad}\boldsymbol{u} - \mathrm{Grad}\boldsymbol{u}_\mathrm{a}] : \mathrm{Grad}\delta\boldsymbol{\lambda} \, \mathrm{d}V = 0 \end{aligned} \tag{29}$$

where $\boldsymbol{S}$ is the (second) Piola-Kirchhoff stress tensor, and

$$\boldsymbol{E} = \frac{1}{2}[\boldsymbol{F}^T \cdot \boldsymbol{F} - \boldsymbol{I}] \tag{30}$$

is the Green-Lagrange strain tensor, the variation of which reads $\delta\boldsymbol{E} = \mathrm{sym}(\boldsymbol{F}^\mathrm{T} \cdot \mathrm{Grad}\delta\boldsymbol{u})$,
where $\mathrm{sym}(\bullet)$ denotes the symmetric part of the second-order tensor.

Linearization of $\delta\boldsymbol{E}$ follows as

$$\mathrm{D}_{\Delta\boldsymbol{u}}\delta\boldsymbol{E} = \mathrm{sym}\left(\mathrm{Grad}^\mathrm{T}\Delta\boldsymbol{u} \cdot \mathrm{Grad}\delta\boldsymbol{u}\right). \tag{31}$$

Linearization of the Lagrangian multipliers' contribution to the non-linear equation Eq. (29) follows as

$$\begin{aligned} \mathrm{D}_{\Delta\boldsymbol{U}}G = & \beta_1 \int_{\Omega_\mathrm{HS}} \Delta\boldsymbol{\lambda} \cdot \delta\boldsymbol{u} \, \mathrm{d}V + \beta_2 \int_{\Omega_\mathrm{HS}} \mathrm{Grad}\,\Delta\boldsymbol{\lambda} : \mathrm{Grad}\delta\boldsymbol{u} \, \mathrm{d}V \\ & + \beta_1 \int_{\Omega_\mathrm{HS}} \Delta\boldsymbol{u} \cdot \delta\boldsymbol{\lambda} \, \mathrm{d}V + \beta_2 \int_{\Omega_\mathrm{HS}} \mathrm{Grad}\Delta\boldsymbol{u} : \mathrm{Grad}\delta\boldsymbol{\lambda} \, \mathrm{d}V, \end{aligned} \tag{32}$$

which is clearly symmetric with respect to $\Delta\boldsymbol{U}$ and $\delta\boldsymbol{U}$.

Following our previous work [10], the material response is governed by the Saint-Venant-Kirchhoff constitutive law

$$\boldsymbol{S} = \mathbb{C} : \boldsymbol{E} \tag{33}$$

where $\mathbb{C}$ is a fourth-order elastic tensor that potentially captures anisotropies arising from a crystal lattice.

The linearisation of Eq. (33) therefore reads

$$\mathrm{D}_{\Delta \boldsymbol{u}} \boldsymbol{S} = \mathbb{C} : \mathrm{sym}(\boldsymbol{F}^{\mathrm{T}} \cdot \mathrm{Grad} \Delta \boldsymbol{u}). \tag{34}$$

5.2. Discretization in space and the resulting system of equations

Finally, we introduce a finite element basis for both virtual and real displacements and Lagrange multipliers

$$\begin{aligned} \boldsymbol{u}(\boldsymbol{X}) &= \sum u^I \boldsymbol{N}^I(\boldsymbol{X}) \\ \boldsymbol{\lambda}(\boldsymbol{X}) &= \sum \lambda^I \boldsymbol{N}^I(\boldsymbol{X}). \end{aligned} \tag{35}$$

where the index I represents a degree-of-freedom and $\boldsymbol{N}^I(\boldsymbol{X})$ is the corresponding vector-valued shape function. The variation and increment of $\boldsymbol{u}$ and $\boldsymbol{\lambda}$ follow as

$$\begin{aligned} \Delta \boldsymbol{u}(\boldsymbol{X}) &= \sum \Delta u^I \boldsymbol{N}^I(\boldsymbol{X}) \\ \delta \boldsymbol{u}(\boldsymbol{X}) &= \sum \delta u^I \boldsymbol{N}^I(\boldsymbol{X}) \\ \Delta \boldsymbol{\lambda}(\boldsymbol{X}) &= \sum \Delta \lambda^I \boldsymbol{N}^I(\boldsymbol{X}) \\ \delta \boldsymbol{\lambda}(\boldsymbol{X}) &= \sum \delta \lambda^I \boldsymbol{N}^I(\boldsymbol{X}). \end{aligned} \tag{36}$$

Requiring that the linearisation of Eq. (29) holds $\forall\ \delta u^I, \delta \lambda^I$, the system of linearized algebraic equations

$$\begin{bmatrix} \mathbf{K}_{cc} & \mathbf{K}_{ch} & \mathbf{0} \\ \mathbf{K}_{hc} & \mathbf{K}_{hh} & \mathbf{G}_{h\lambda} \\ \mathbf{0} & \mathbf{G}_{\lambda h} & \mathbf{0} \end{bmatrix} \begin{bmatrix} \Delta \mathbf{u}_c \\ \Delta \mathbf{u}_h \\ \Delta \boldsymbol{\lambda} \end{bmatrix} = \begin{bmatrix} \mathbf{F}_c \\ \mathbf{F}_h \\ \mathbf{F}_\lambda \end{bmatrix} \quad , \qquad \mathbf{K} = \begin{bmatrix} \mathbf{K}_{cc} & \mathbf{K}_{ch} \\ \mathbf{K}_{hc} & \mathbf{K}_{hh} \end{bmatrix} \tag{37}$$

where

$$\mathrm{K}^{IJ} = \int_{\Omega_\mathrm{c}} [\boldsymbol{F}^T \cdot \mathrm{Grad}\boldsymbol{N}^I] : \mathbb{C} : [\boldsymbol{F}^T \cdot \mathrm{Grad}\boldsymbol{N}^J] + \boldsymbol{S} : [\mathrm{Grad}^T\boldsymbol{N}^J \cdot \mathrm{Grad}\boldsymbol{N}^I]\,\mathrm{d}V \tag{38}$$

$$\mathrm{G}^{IJ}_{h\lambda} = \mathrm{G}^{JI}_{\lambda h} = \beta_1 \int_{\Omega_\mathrm{c}} \boldsymbol{N}^I \cdot \boldsymbol{N}^J\,\mathrm{d}V + \beta_2 \int_{\Omega_\mathrm{c}} \mathrm{Grad}\boldsymbol{N}^I : \mathrm{Grad}\boldsymbol{N}^J\,\mathrm{d}V$$

$$\mathrm{F}^I_c = \int_{\Omega_\mathrm{c}} \boldsymbol{B} \cdot \boldsymbol{N}^I\,\mathrm{d}V + \int_{\partial\Omega^\sigma_\mathrm{c}} \overline{\boldsymbol{T}} \cdot \boldsymbol{N}^I\,\mathrm{d}S - \int_{\Omega_\mathrm{c}} \boldsymbol{S} : \delta\boldsymbol{E}^I\,\mathrm{d}V \tag{39}$$

$$\mathrm{F}^I_h = \int_{\Omega_\mathrm{c}} \boldsymbol{B} \cdot \boldsymbol{N}^I\,\mathrm{d}V + \int_{\partial\Omega^\sigma_\mathrm{c}} \overline{\boldsymbol{T}} \cdot \boldsymbol{N}^I\,\mathrm{d}S - \int_{\Omega_\mathrm{c}} \boldsymbol{S} : \delta\boldsymbol{E}^I\,\mathrm{d}V \tag{40}$$

$$- \beta_1 \int_{\Omega_\mathrm{HS}} \boldsymbol{\lambda} \cdot \boldsymbol{N}^I\,\mathrm{d}V - \beta_2 \int_{\Omega_\mathrm{HS}} \mathrm{Grad}\boldsymbol{\lambda} : \mathrm{Grad}\boldsymbol{N}^I\,\mathrm{d}V \tag{41}$$

$$\mathrm{F}^I_\lambda = \beta_1 \int_{\Omega_\mathrm{HS}} [\boldsymbol{u}_\mathrm{a} - \boldsymbol{u}] \cdot \boldsymbol{N}^I\,\mathrm{d}V + \beta_2 \int_{\Omega_\mathrm{HS}} [\mathrm{Grad}\boldsymbol{u}_\mathrm{a} - \mathrm{Grad}\boldsymbol{u}] : \mathrm{Grad}\boldsymbol{N}^I\,\mathrm{d}V$$

is obtained. The quantity $\Delta\mathbf{u}_c$ denotes those degrees-of-freedom that lie in $\Omega/\Omega_\mathrm{HS}$, whereas $\Delta\mathbf{u}_h$ corresponds to those in the handshake region Ω_HS, and $\delta\boldsymbol{E}^I = \mathrm{sym}(\boldsymbol{F}^\mathrm{T} \cdot \mathrm{Grad}\delta\boldsymbol{N}^\mathrm{I})$.

Note that we consider the case when $\Omega_\mathrm{HS} \cap \partial\Omega^\mathrm{u}_\mathrm{c} = \emptyset$, that is to say that the Dirichlet boundary conditions are applied to the "outer" boundary of the continuum domain where no Lagrange multipliers are defined. The alternative case would require additional attention. In particular, the sparsity pattern of the resulting matrices would need to take into account Dirichlet boundary conditions to exclude the prescribed degrees-of-freedom from the system of equations. Otherwise, the condensation of the resulting matrix may result in some rows of $G_{\lambda h}$ (and columns of $G_{h\lambda}$) being completely zero, rendering the resulting matrix noninvertible.

Each of the coupling strategies follow as a special case to this formulation. When we remove all blocks in the resulting matrix and vectors associated with the Lagrange multiplier field and apply atomistic Dirichlet boundary conditions on $\partial\Omega^\mathrm{a}_\mathrm{c}$ together with the prescribed Dirichlet boundary conditions on $\partial\Omega^\mathrm{l}_\mathrm{c} \cup \partial\Omega^\mathrm{r}_\mathrm{c} \cup \partial\Omega^\mathrm{b}_\mathrm{c} \cup \partial\Omega^\mathrm{t}_\mathrm{c}$, we obtain the surface-type displacement coupling method. Using a similar approach but replacing the Dirichlet conditions with Neumann boundary conditions leads to the surface-type traction coupling method. The volume coupling method which minimizes the point-wise difference between the continuum displacement field and the atomistic displacements follows after the substitution of the integrals with β_1 by a sum over all particles in Ω_HS and dropping terms associated with β_2. This can be considered as a specific quadrature integration rule, that is different for each cell.

5.3. Schur compliment and preconditioners for iterative solvers

The solution of the system Eq. (37) is obtained by forming the Schur compliment. By multiplying the first equation

$$\mathbf{K}_{cc} \cdot \Delta \mathbf{u}_c + \mathbf{K}_{ch} \cdot \Delta \mathbf{u}_h = \mathbf{F}_c \tag{42}$$

with $\mathbf{K}_{hc} \cdot \mathbf{K}_{cc}^{-1}$ from the left and subtracting the second equation we obtain

$$\underbrace{[\mathbf{K}_{hc} \cdot \mathbf{K}_{cc}^{-1} \cdot \mathbf{K}_{ch} - \mathbf{K}_h]}_{\tilde{\mathbf{K}}_h} \cdot \Delta \mathbf{u}_h - \mathbf{G}_{h\lambda} \cdot \Delta \boldsymbol{\lambda} = \mathbf{K}_{hc} \cdot \mathbf{K}_{cc}^{-1} \cdot \mathbf{F}_c - \mathbf{F}_h =: \tilde{\mathbf{F}}_h. \tag{43}$$

Next, multiplication with $\mathbf{G}_{\lambda h} \cdot \tilde{\mathbf{K}}_h^{-1}$ from the left and subtraction of the third equation in Eq. (37) leads to

$$\underbrace{\mathbf{G}_{\lambda h} \cdot \tilde{\mathbf{K}}_h^{-1} \cdot \mathbf{G}_{h\lambda}}_{\tilde{\mathbf{K}}_\lambda} \Delta \boldsymbol{\lambda} = \mathbf{F}_\lambda - \mathbf{G}_{\lambda h} \cdot \tilde{\mathbf{K}}_h^{-1} \cdot \tilde{\mathbf{F}}_h := \tilde{\mathbf{F}}_\lambda. \tag{44}$$

Since $\mathbf{K}_{cc}$ and $\mathbf{K}_{hh}$ are symmetric positive-definite matrices and $\mathbf{K}_{ch} = \mathbf{K}_{ch}^T$ has full column rank, $\tilde{\mathbf{K}}_h$ is also positive-definite. Similarly, $\mathbf{G}_{\lambda h} = \mathbf{G}_{\lambda h}^T$ has full column rank and $\tilde{\mathbf{K}}_\lambda$ is positive-definite.

Note that although both $\tilde{\mathbf{K}}_h$ and $\tilde{\mathbf{K}}_\lambda$ are full matrices, for use with solution procedures utilizing iterative solvers they need not be directly computed and stored, but can rather be considered as linear operators acting on vectors.

We consider the case when the same basis functions are used to discretize the Lagrange multipliers and the displacements in Ω_{HS}. This leads to $\mathbf{G}_{\lambda h}$ being square and invertible. For the L_2 coupling method this is equivalent to the mass matrix on Ω_{HS}. Therefore, the outer Schur compliment can be solved by multiplying Eq. (44) with $\mathbf{G}_{\lambda h}^{-1} \cdot \tilde{\mathbf{K}}_h \cdot \mathbf{G}_{h\lambda}^{-1}$ which leads to

$$\Delta \boldsymbol{\lambda} = \mathbf{G}_{\lambda h}^{-1} \cdot [\tilde{\mathbf{K}}_h \cdot \mathbf{G}_{h\lambda}^{-1} \cdot \mathbf{F}_\lambda - \tilde{\mathbf{F}}_h]. \tag{45}$$

For the application of $\mathbf{G}_{\lambda h}^{-1}$ to a vector, the SSOR preconditioner was utilized in conjunction with the Conjugate Gradient (CG) method. Knowing $\Delta \boldsymbol{\lambda}$, Eq. (43) can be solved for $\Delta \mathbf{u}_h$. To achieve this, we form the corresponding RHS ($\tilde{\mathbf{F}}_h$). To form a preconditioner to $\tilde{\mathbf{K}}_h$ we do the following: First, $\tilde{\mathbf{K}}_h$ is approximated by $\tilde{\mathbf{K}}_h \approx \mathbf{K}_{hc} \cdot \mathbf{D}_{cc}^{-1} \cdot \mathbf{K}_{ch} - \mathbf{K}_h := \overline{\mathbf{K}}_h$, where $\mathbf{D}_{cc}$ is a diagonal part of $\mathbf{K}_{cc}$. Next, the action of the preconditioner on a vector $\mathbf{y}$ is considered to be the solution of the $\overline{\mathbf{K}}_h \cdot \mathbf{x} = \mathbf{y}$ using the CG method with a low number of iterations. Finally, Eq. (42) is solved for $\Delta \mathbf{u}_c$. The SSOR preconditioner was also used in the inversion of $\mathbf{K}_{cc}$ and in the definition of the inner Schur compliment $\tilde{\mathbf{K}}_h$.

6. Numerical examples

In the following examples we consider a FCC crystal of copper. On the atomistic side it is modelled using the EAM potential given by Foiles et al. [16], which has the lattice parameter $a = 3.615$A at zero temperature and the cut-off radius 4.94A. Atomistic simulations are performed using the LAMMPS open-source software [43]. The continuum formulation has been implemented using the open-source deal.II[4] FEM library.

The quartic averaging kernel of radius R was used (Fig. 2) to evaluate the continuum fields from the atomistic simulations. Its analytical expression is given by

$$w(r) = \frac{35}{8\,V}\,[1 - r^2]^2 \tag{46}$$

with $r = |\mathbf{X}^\alpha - \boldsymbol{X}|/R_w$ and $V = \frac{4}{3}\pi R_w^3$. If not mentioned otherwise, all the results are obtained with averaging radius R_w equal to 9A.

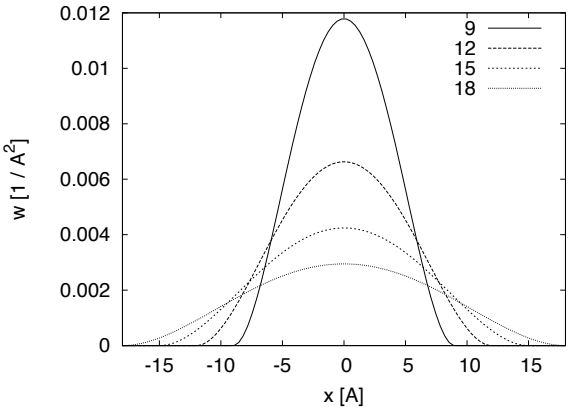

Figure 2: Quartic kernels of different averaging (smoothing) radius.

In our implementation we employed the following mechanisms to speed-up stress fields calculation: Firstly, we consider only those particles α for which $|\mathbf{X}^\alpha - \boldsymbol{X}_I| \leq R_w + R_c$, where R_c is the maximum cut-off distance for the here considered two-point EAM potential and R_w is the radius of the averaging kernel. In other words, if this condition is not satisfied there is no particle β with which α interacts (i.e. $\mathbf{f}^{\alpha\beta} \neq \mathbf{o}$) such that the corresponding bond is non-zero $\widehat{w}^{\alpha\beta}(\boldsymbol{X}_I, \mathbf{X}^\alpha, \mathbf{X}^\beta) \neq 0$. Secondly, we limit the atoms considered for field calculations during staggered coupling schemes to particles for which $\mathbf{X}^\alpha \in \Omega_{\mathrm{HS}} \cup \Omega_{\mathrm{a/c}} \cup \Omega_{\mathrm{ap}}$. Finally, bond values were cached during calculations. The calculation of kinematic quantities was also accelerated by

considering for each node I only such particles $\alpha : |\mathbf{X}^{\alpha} - \boldsymbol{X}_I| \leq R_w$. Other particles, obviously, do not contribute to the value of the field evaluated at a particular node I.

The cubic anisotropy continuum parameters are taken from our previous studies [9] as: $C_{11} = 167.26$ GPa, $C_{12} = 124.15$ GPa, $C_{44} = 76.44$ GPa.

All results are obtained with the mesh depicted in Fig. 1(b), which was created with the Gmsh meshing program [17]. From the atomistic simulation point of view, a square plate is oriented along the crystallographic axes. The number of unit cells in the third dimension was fixed to 4, whereas in the two other dimensions was set to 140 to be comparable with our previous studies [10]. In the numerical example with a hole, the ratio between the diameter of the hole and the width of the plate is kept equal to 1/5. The side length of the domains $\Omega_{\mathrm{a}'}$, Ω_{ap}, Ω_{HS}, $\Omega_{\mathrm{a/c}}$ and Ω_{p} are 80, 74, 60, 46 and 32 unit cells respectively. All atomistic simulations were performed with periodic boundary conditions in the third dimension.

For coupling methods which include Lagrange multipliers, the following constants were used: For the discrete displacement (volume-type) coupling method (denoted in figures as λ_δ) and for the continuous displacement (volume-type) coupling method with L_2 norm (denoted in figures as λ_{L_2}), $\beta_1 = C_{11}$ is specified. For the continuous displacement (volume-type) coupling with H_1 norm (denoted in figures as λ_{H_1}), $\beta_1 = 2C_{11}/V(\Omega_{\mathrm{c}}/\Omega_{\mathrm{HS}})$ and $\beta_2 = C_{11}$ are employed as an attempt to generalize the optimal values of these constants reported in [5] for a one-dimensional Arlequin method. The surface-type coupling displacement method is denoted by U_{a} and the surface-type coupling traction method is denoted by T_{a}.

Lagrange-multipliers fields are introduced for the corresponding coupling methods in the Ω_{HS} region. $Q1$ basis functions are used for the continuum formulation. The left, right, bottom and top parts of the continuum domain where the displacement boundary conditions are to be applied are denoted by $\partial\Omega_{\mathrm{c}}^{\mathrm{l}}$, $\partial\Omega_{\mathrm{c}}^{\mathrm{r}}$, $\partial\Omega_{\mathrm{c}}^{\mathrm{b}}$, $\partial\Omega_{\mathrm{c}}^{\mathrm{t}}$ respectively. The boundary of the continuum domain used for the strong coupling is denoted by $\partial\Omega_{\mathrm{c}}^{\mathrm{a}}$. Surface-type coupling methods impose on this boundary either traction or displacement boundary conditions based on fields calculated from the atomistic simulation.

6.1. Averaging radius convergence

This section serves as a benchmark used to evaluate the Lagrangian averaging approach for calculating the local (microscopic) continuum quantities from the atomistic simulations.

Consider a RVE (Fig. 3(a)) modelled solely with MM under periodic boundary conditions under uniaxial loading for which the applied macroscopic deformation

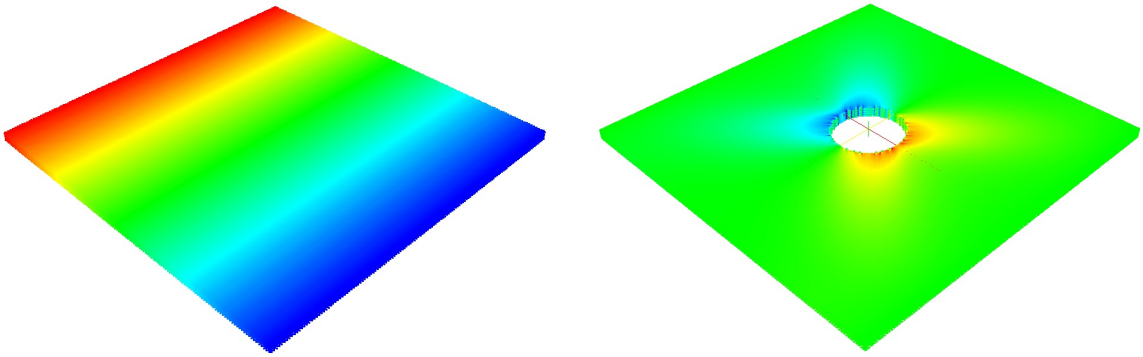

(a) Uniaxial (b) Surface tension

Figure 3: Particles displacements in a plate in x direction as obtained from the fully resolved atomistic simulations with periodic RVEs. (a): homogeneous plate with a uniaxial stretch of 1.0003951; (b): plate with a hole relaxed under surface tension.

gradient is

$$\boldsymbol{F} = \begin{bmatrix} F_{11} & 0 \\ 0 & 1 \end{bmatrix}, \tag{47}$$

which is produced through an affine displacement of all atoms. No additional energy minimization step is required for the case of homogeneous deformation of a simple crystal. The dependence of the continuum fields obtained from the atomistic simulations on the radius of the averaging kernel (Fig. 2) is studied for the unstructured mesh illustrated in Fig. 1(b). To the best of our knowledge, only structured grids have been used by other researchers. Utilizing unstructured meshes may lead to the deterioration of the quality of fields calculated using averaging techniques.

To this end we compare continuum fields (displacement, deformation gradient, Cauchy stress) evaluated at each grid point from the atomistic simulation to the macroscopic counterparts, namely the macroscopic deformation gradient, macroscopic stress (which equals the Virial pressure taken with an opposite sign [11]) and the applied affine displacement. The results are presented in Fig. 4.

From this data, several observations can be made. For the quartic averaging kernel applied to copper, the resulting displacement fields are the most accurate and have the least noise (scatter) as compared to other fields for the same averaging radius. The Cauchy stress obtained via Eq. (4) and Eq. (5) is the least accurate and has the most noise. The reason for this is most likely the calculation of the integral in Eq. (6) which depends on the intersection of the interparticle vector distance $\mathbf{X}^{\alpha\beta}$ and the averaging kernel. Consequently when applied to general problems we expect

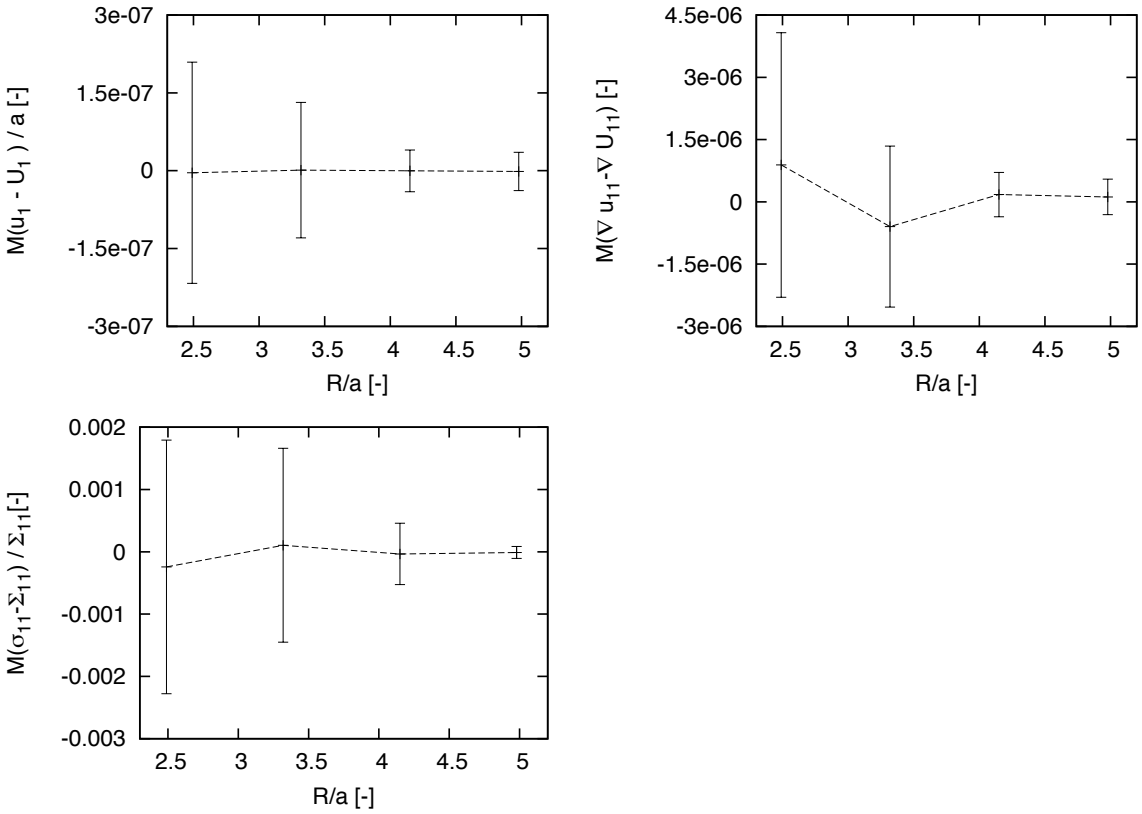

Figure 4: The convergence of continuum fields as evaluated from pure atomistic solution under uniaxial deformation and with periodic boundary conditions. Mean values and standard deviations of the difference between obtained and the expected values are shown. Values are given in dimensionless form with $a = 3.615$, the macroscopic Cauchy stress $\Sigma_{11} = 0.066$ GPa and the macroscopic deformation gradient $\nabla \mathrm{U}_{11} = 3.952\ 10^{-4}$.

to have more variation in kinetic quantities (stresses) as compared to kinematic ones (displacement, deformation gradient).

Overall, the quality of the results obtained using the atomistic-to-continuum correspondence principle is good.

6.2. Patch test

Next, we study the four staggered coupling strategies described in Section 4 for the same problem, namely uniaxial deformation of a plate. Continuum and atomistic domains are considered as described in caption of Fig. 1(a). On $\partial\Omega_{\mathrm{c}}^{\mathrm{l}}$ and

$\partial\Omega_c^r$ displacement in x direction of equal value and opposite sign is prescribed, while on $\partial\Omega_c^b$ and $\partial\Omega_c^t$ displacement in y direction is prescribed to be zero. Results of the patch test for different coupling strategies are presented in Fig. 5.

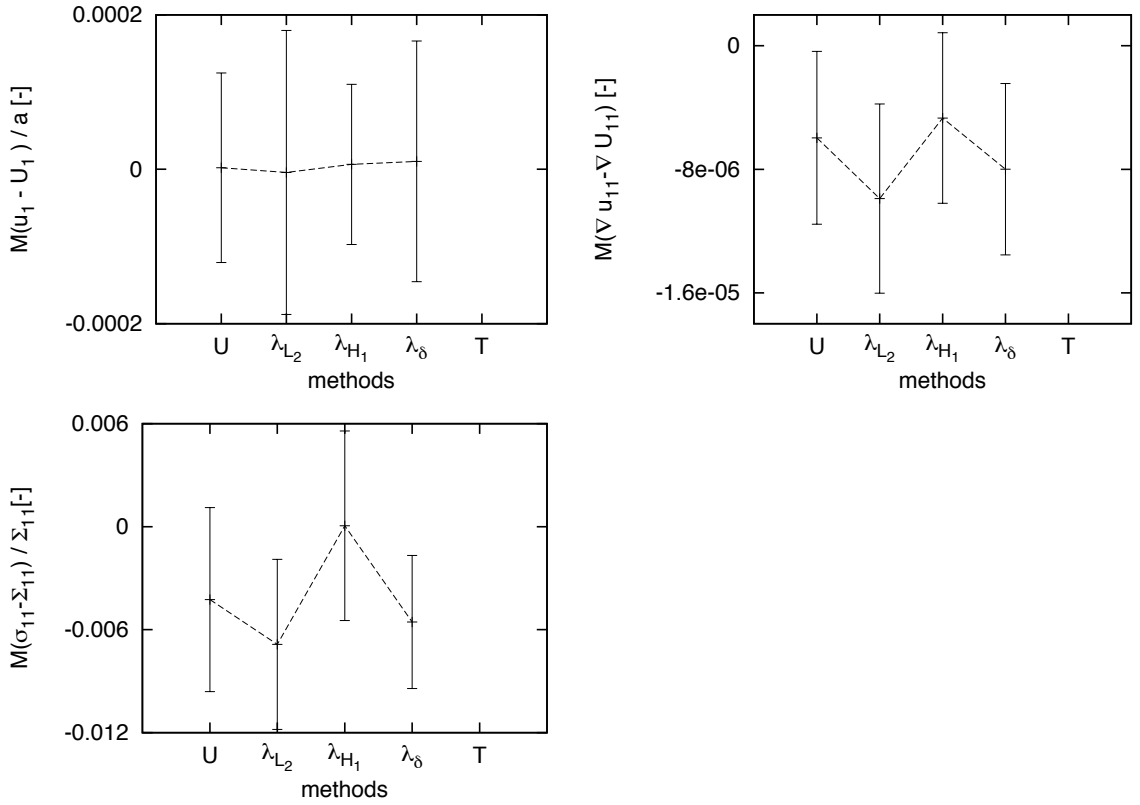

Figure 5: Convergence of continuum fields as evaluated from the atomistic domain for different coupling strategies under uniaxial deformation gradient. Fields obtained in a part of the atomistic domain ($\Omega_h \cup \Omega_{a'} \cup \Omega_{ap} \cup \Omega_{HS}$) are compared to the analytical solution in terms of the mean error and its standard deviation.

Firstly, it should be noted that the traction surface-type coupling method did not converge for a simple patch problem. As we will see later, it will work for the plate with a hole problem, but will not be the best performer. In terms of scatter, the other four coupling methods are almost identical. The accuracy in terms of the resulting displacement field is approximately the same. However, in terms of kinetic quantities, the H_1 volume-type coupling method performs best. This is to be expected as displacement gradients are used to form a strain measure (Eq. (30)) which is directly connected to the stress field through the constitutive equation (Eq.

(33)).

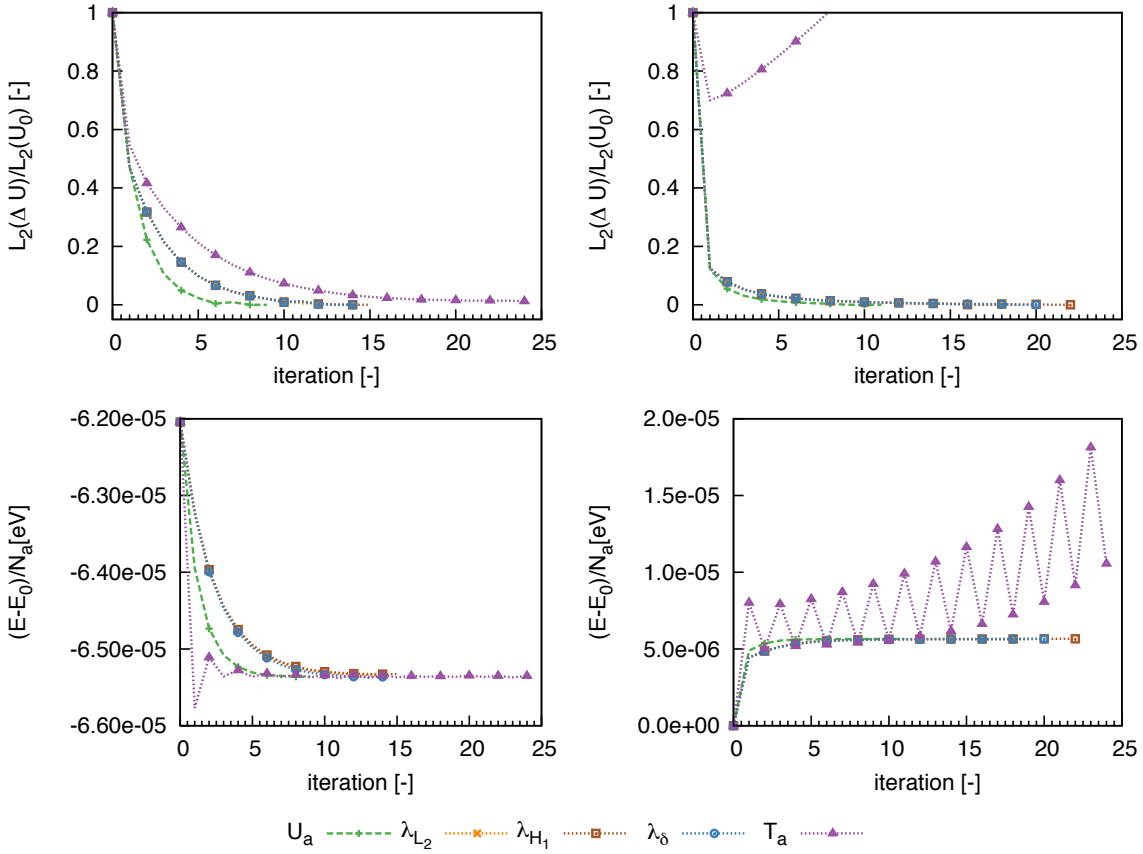

Figure 6: Convergence of atomistic and continuum solutions for different coupling schemes. Left: plate with a hole; Right: uniaxial tension. Coupling methods are denoted as follows: strong displacement $\mathrm{U_a}$, strong traction $\mathrm{T_a}$, weak H_1 Lagrange multipliers $\lambda_{\mathrm{H_1}}$, weak L_2 Lagrange multipliers $\lambda_{\mathrm{L_2}}$, weak Lagrange multipliers based on delta-distribution λ_δ.

Apart from the traction coupling method, the convergence rates of all coupling methods (Fig. 6 right) for the patch test are almost identical. Overall, it can be concluded that the coupling methods, as applied to the patch test, are accurate.

6.3. Plate with a hole

Finally, we move to a numerical example with a non-homogeneous solution, namely that of a 2d plate with a hole relaxed under surface tension as is illustrated in Fig. 3(b). All atoms within the domain Ω_h are removed from the perfect lattice

configuration. Due to the missing neighbours, the system is no longer in equilibrium and minimization of the total energy results in the displacement of atoms.

For this example there is no analytical solution available, thus in addition to the five coupling strategies considered, we add a fully resolved atomistic solution and denote it by A in the figures. As another point of comparison, we plot the local fields obtained from the surface enhanced continuum theory (SEC) [19], which we successfully applied in our previous studies [9]. As explained in [9], the parameters to the SEC were determined by fitting the macroscopic size effect.

The local Cauchy stresses, displacements and displacement gradients from the atomistic, SEC and coupled approaches are compared in Figs. 7 and 8. The results were evaluated along the lines $x = 0$ and $y = 0$. Due to the symmetry of the problem we do not plot all components of fields, but only those which are different. For example, it is sufficient to report $\sigma_{11}(x)$, which equals $\sigma_{22}(y)$.

We defer the discussion of the results until the next section, noting only that the strong traction coupling method did converge for a plate with a hole.

7. Discussion and Conclusions

From the numerical results obtained in the previous section we can draw several conclusions.

First of all, the method based on the traction (surface-type) coupling is not robust, at least for the studied problems and FCC material. Although it did converge for a more complicated example of a plate with a hole, it failed to reproduce a simple patch test of uniaxial deformation[8]. In any case, the usage of tractions as boundary conditions relies on the evaluation of the Piola stress at appropriate nodes. This operation is considerably more resource consuming than the kinematic fields since it involves the double loop over the particles and calculation of a bond integral for each pair of interacting particles and each node of interest (Eqs. 5 and 6). Given all performance enhancing measures, the kinetic calculations still took considerably more time as compared to kinematic calculations. Thus, staggered coupling schemes based on kinematic coupling are generally more efficient from a computational perspective. In particular, the surface-type displacement coupling method is the most efficient given the fact that there is no need to form the Schur-compliment on the continuum side. Rather, the resulting system of equations can be solved right away using any iterative solver, such as the CG solver.

[8]During development of this work the traction-based coupling method was however successfully applied to a 1d deformation of a bar.

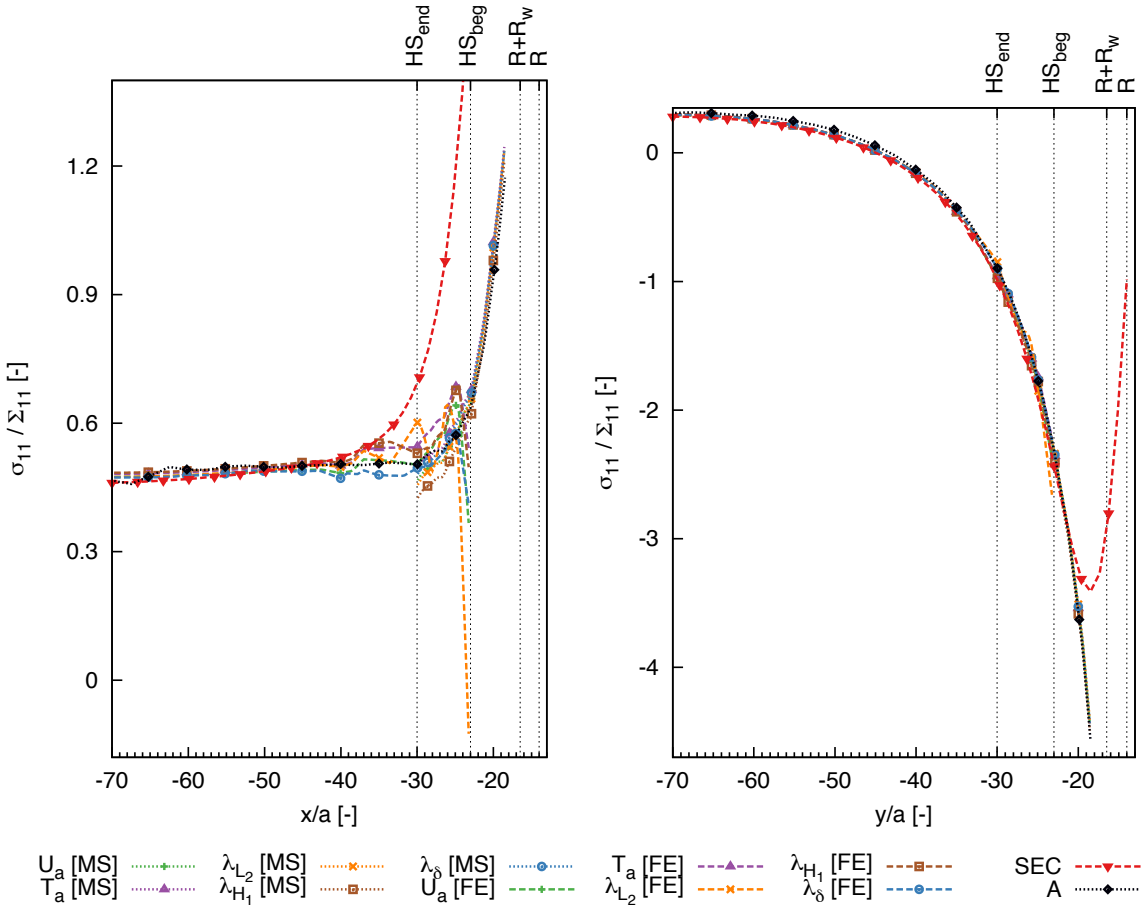

Figure 7: A comparison of kinetic quantities (Cauchy stress) as calculated from the atomistic and continuum approaches for the plate with a hole relaxed under surface tension. The macroscopic stress calculated from the fully-resolved atomistic simulation equals $\Sigma_{11} = 0.02892$ GPa. Coupling methods are denoted as follows: strong displacement $\mathrm{U_a}$, strong traction $\mathrm{T_a}$, weak H_1 Lagrange multipliers $\lambda_{\mathrm{H_1}}$, weak L_2 Lagrange multipliers $\lambda_{\mathrm{L_2}}$, weak Lagrange multipliers based on delta-distribution λ_δ. The suffixes [MS] and [FE] denote fields obtained from atomistic and continuum sides of the coupled problem, respectively. R and R_w denote the radius of the hole and the averaging kernel, respectively. HS_{beg} and HS_{end} indicate beginning and end of the handshaking region.

For the simple case of uniaxial deformation, the convergence rates of all coupling methods, excluding that which is traction-based, are almost identical. This, however,

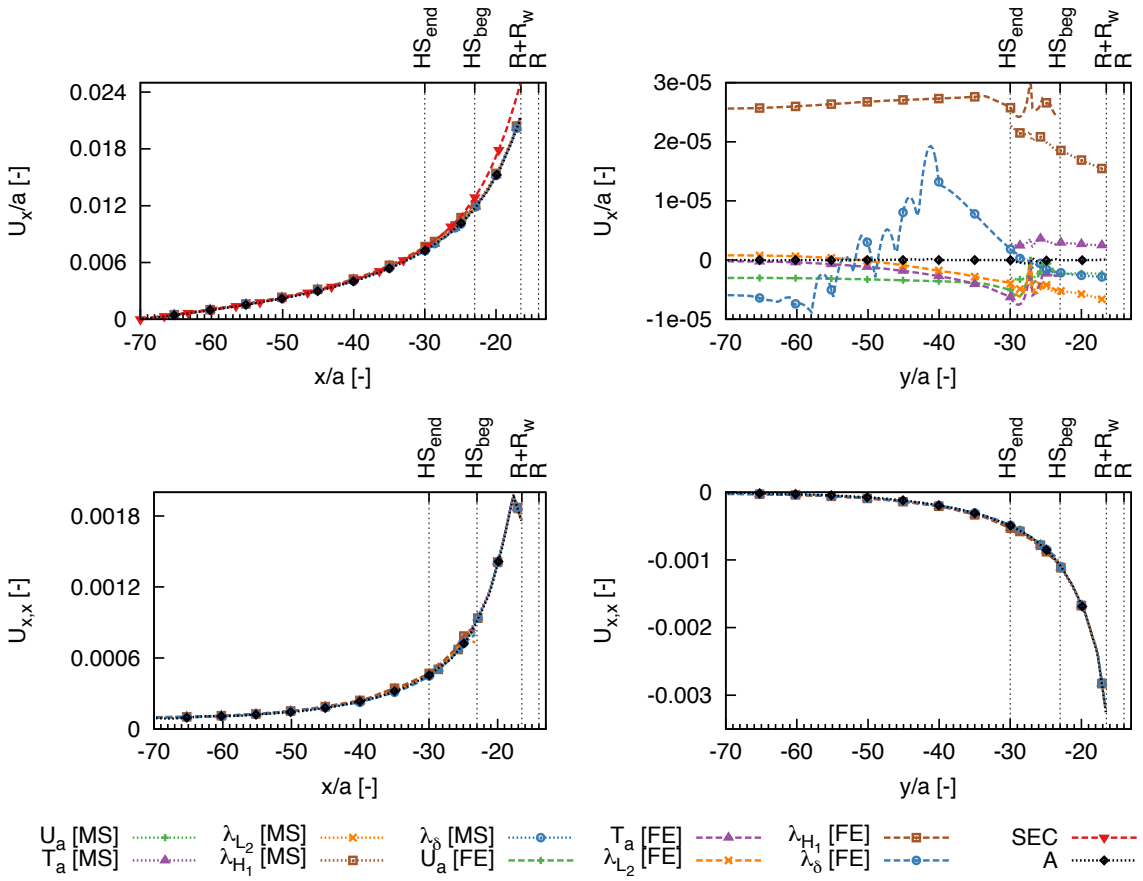

Figure 8: A comparison of kinematic quantities (displacements, deformation gradient) as calculated from the atomistic and continuum approaches for the plate with a hole relaxed under the surface tension. Coupling methods are denoted as follows: strong displacement $\mathrm{U_a}$, strong traction $\mathrm{T_a}$, weak H_1 Lagrange multipliers $\lambda_{\mathrm{H_1}}$, weak L_2 Lagrange multipliers $\lambda_{\mathrm{L_2}}$, weak Lagrange multipliers based on delta-distribution λ_δ. The suffixes [MS] and [FE] denote fields obtained from atomistic and continuum sides of the coupled problem, respectively. R and R_w denote the radius of the hole and the averaging kernel, respectively. HS_{beg} and HS_{end} indicate beginning and end of the handshaking region.

does change for the case of a plate with a hole, where the surface-type displacement boundary condition coupling method converges faster than the other methods and is therefore preferable from this perspective.

The accuracy of the coupling methods were assessed by comparing the results for

the patch test to its analytical solution, and the coupled results for the plate with a hole problem to those obtained from the fully resolved atomistic simulation. In terms of the first test problem, the preferred methods are the displacement (surface-type) coupling and the H_1 displacement (volume-type) coupling. For the plate with a hole problem, the coupling methods studied here show the most difference in terms of kinetic quantities, and in particular $\sigma_{11}(x)$. Overall, the best performance was obtained using the displacement (surface-type) coupling method, the discrete displacements (volume-type) coupling method and the H_1 continuous displacement (volume-type) coupling method. Comparatively, the coupling strategies considered here produce rather similar results. These could likely be made more accurate if other factors such as the size of Ω_{HS}, the mesh size, constants β_1 and β_2 and the like are adjusted. It is worth noting that the coupled formulation, although not perfect, produced results closer to the fully-resolved atomistic simulation when compared to the SEC.

In this paper we have studied different staggered coupling strategies based on the atomistic-to-continuum correspondence. While developing the theoretical formulation, similarities to other methods proposed in the literature have been given. Our implementation was based on two robust C++ libraries, namely LAMMPS [43] for molecular statics simulations, and deal.II [4] for solving the partial differential equations of continuum mechanics. The latter also provided an infrastructure to calculate and use fields from the atomistic simulation. Both parts of the implementation are very general and can be applied to domains of arbitrary geometry and meshes.

In a future work we would like to apply the averaging procedure to polymer systems with nano-particles and to calculate local fields. The coupling strategies considered here will be generalized to finite temperatures in a manner similar to [42, 46].

Acknowledgements

The financial support of the German Science Foundation (Deutsche Forschungs-Gemeinschaft, DFG), grant STE 544/46-1, is gratefully acknowledged. The support of this work by the ERC Advanced Grant MOCOPOLY is gratefully acknowledged by the second and third authors.

The first author is also grateful to Wolfgang Bangerth and Timo Heister for discussing in the on-line forum several implementation details using deal.II library.

References

[1] Abraham, F. F., Broughton, J. Q., Bernstein, N., Kaxiras, E., Dec. 1998. Spanning the continuum to quantum length scales in a dynamic simulation of brittle

fracture. EPL (Europhysics Letters) 44 (6), 783–6.

[2] Anciaux, G., Ramisetti, S. B., Molinari, J. F., 2012. A finite temperature bridging domain method for MD-FE coupling and application to a contact problem. Computer Methods in Applied Mechanics and Engineering 205-208 (1), 204–212.

[3] Ariza, M. P., Romero, I., Ponga, M., Ortiz, M., Dec. 2011. HotQC simulation of nanovoid growth under tension in copper. International Journal of Fracture 174 (1), 75–85.

[4] Bangerth, W., Hartmann, R., Kanschat, G., Aug. 2007. deal.II—A general-purpose object-oriented finite element library. ACM Transactions on Mathematical Software 33 (4), 24–es.

[5] Bauman, P. T., Dhia, H. B., Elkhodja, N., Oden, J. T., Prudhomme, S., May 2008. On the application of the Arlequin method to the coupling of particle and continuum models. Computational Mechanics 42 (4), 511–530.

[6] Bauman, P. T., Oden, J. T., Prudhomme, S., Jan. 2009. Adaptive multiscale modeling of polymeric materials with Arlequin coupling and Goals algorithms. Computer Methods in Applied Mechanics and Engineering 198 (5-8), 799–818.

[7] Belytschko, T., Xiao, S., May 2003. Coupling methods for continuum model with molecular model. International Journal for Multiscale Computational Engineering 1 (1), 115–126.

[8] Broughton, J. Q., Abraham, F. F., Bernstein, N., Kaxiras, E., Jul. 1999. Concurrent coupling of length scales: Methodology and application. Physical Review B 60, 2391–2403.

[9] Davydov, D., Javili, A., Steinmann, P., 2013. On molecular statics and surface-enhanced continuum modeling of nano-structures. Computational Materials Science 69, 510–519.

[10] Davydov, D., Javili, A., Steinmann, P., McBride, A., Dec. 2012. A Comparison of Atomistic and Surface Enhanced Continuum Approaches at Finite Temperature. In: Altenbach, H., Morozov, N. F. (Eds.), Surface Effects in Solid Mechanics. Springer Verlag, pp. 1–15.

[11] Davydov, D., Steinmann, P., 2013. Reviewing the roots of continuum formulations in molecular systems. Part I: Particle dynamics, statistical physics, mass

and linear momentum balance equations. Mathematics and Mechanics of Solids, 1–23.

[12] Davydov, D., Steinmann, P., 2013. Reviewing the roots of continuum formulations in molecular systems. Part II: Energy and Angular Momentum Balance Equation. Mathematics and Mechanics of Solids, 1–16.

[13] Davydov, D., Steinmann, P., 2013. Reviewing the roots of continuum formulations in molecular systems. Part III: Stresses, Couple Stresses, Heat Fluxes. Submitted.

[14] Dupuy, L., Tadmor, E. B., Miller, R. E., Phillips, R., Aug. 2005. Finite-Temperature Quasicontinuum: Molecular Dynamics without All the Atoms. Physical Review Letters 95 (6), 060202.

[15] Fish, J., Nuggehally, M. A., Shephard, M. S., Picu, C. R., Badia, S., Parks, M. L., Gunzburger, M., Sep. 2007. Concurrent AtC coupling based on a blend of the continuum stress and the atomistic force. Computer Methods in Applied Mechanics and Engineering 196 (45-48), 4548–4560.

[16] Foiles, S. M., Baskes, M. I., Daw, M. S., 1986. Embedded-atom-method functions for the fcc metals Cu, Ag, Au, Ni, Pd, Pt, and their alloys. Physical Review B 33 (12), 7983–7991.

[17] Geuzaine, C., Remacle, J.-F., Sep. 2009. Gmsh: A 3-D finite element mesh generator with built-in pre- and post-processing facilities. International Journal for Numerical Methods in Engineering 79 (11), 1309–1331.

[18] Irving, J. H., Kirkwood, J. G., 1950. The Statistical Mechanical Theory of Transport Processes. IV. The Equations of Hydrodynamics. The Journal of Chemical Physics 18 (6), 817–829.

[19] Javili, A., Steinmann, P., May 2009. A finite element framework for continua with boundary energies. Part I: The two-dimensional case. Computer Methods in Applied Mechanics and Engineering 198 (27-29), 2198–2208.

[20] Karpov, E. G., Park, H. S., Liu, W. K., 2007. A phonon heat bath approach for the atomistic and multiscale simulation of solids. International Journal for Numerical Methods in Engineering 70 (3), 351–378.

[21] Karpov, E. G., Wagner, G. J., Liu, W. K., 2005. A Green's function approach to deriving non-reflecting boundary conditions in molecular dynamics simulations. International Journal for Numerical Methods in Engineering 62 (9), 1250–1262.

[22] Klein, P. A., Zimmerman, J. A., 2006. Coupled atomistic-continuum simulations using arbitrary overlapping domains. Journal of Computational Physics 213 (1), 86–116.

[23] Kulkarni, Y., KNAP, J., Ortiz, M., Apr. 2008. A variational approach to coarse graining of equilibrium and non-equilibrium atomistic description at finite temperature. Journal of the Mechanics and Physics of Solids 56 (4), 1417–1449.

[24] Li, S., Liu, X., Agrawal, A., To, A. C., Jul. 2006. Perfectly matched multiscale simulations for discrete lattice systems: Extension to multiple dimensions. Physical Review B 74 (4), 045418.

[25] Li, S., Sheng, N., Aug. 2010. On multiscale non-equilibrium molecular dynamics simulations. International Journal for Numerical Methods in Engineering 83 (8-9), 998–1038.

[26] Li, X., Dec. 2008. Variational boundary conditions for molecular dynamics simulations: Treatment of the loading condition. Journal of Computational Physics 227 (24), 10078–10093.

[27] Li, X., Sep. 2009. Efficient boundary conditions for molecular statics models of solids. Physical Review B 80 (10), 104112.

[28] Li, X., E, W., Jul. 2005. Multiscale modeling of the dynamics of solids at finite temperature. Journal of the Mechanics and Physics of Solids 53 (7), 1650–1685.

[29] Li, X., E, W., Sep. 2007. Variational boundary conditions for molecular dynamics simulations of crystalline solids at finite temperature: Treatment of the thermal bath. Physical Review B 76 (10), 104107.

[30] Li, X., Yang, J. Z., E, W., May 2010. A multiscale coupling method for the modeling of dynamics of solids with application to brittle cracks. Journal of Computational Physics 229 (10), 3970–3987.

[31] Liu, W. K., Karpov, E. G., Zhang, S., Park, H. S., May 2004. An introduction to computational nanomechanics and materials. Computer Methods in Applied Mechanics and Engineering 193 (17-20), 1529–1578.

[32] Liu, W. K., Qian, D., Gonella, S., Li, S., Chen, W., Chirputkar, S. U., Aug. 2010. Multiscale methods for mechanical science of complex materials: Bridging from quantum to stochastic multiresolution continuum. International Journal for Numerical Methods in Engineering 83 (8-9), 1039–1080.

[33] Lu, G., Tadmor, E. B., Kaxiras, E., Jan. 2006. From electrons to finite elements: A concurrent multiscale approach for metals. Physical Review B 73 (2), 024108.

[34] Mathew, N., Picu, R. C., Bloomfield, M., Jan. 2011. Concurrent coupling of atomistic and continuum models at finite temperature. Computer Methods in Applied Mechanics and Engineering 200 (5-8), 765–773.

[35] Miller, R. E., Tadmor, E. B., May 2009. A unified framework and performance benchmark of fourteen multiscale atomistic/continuum coupling methods. Modelling and Simulation in Materials Science and Engineering 17 (5), 053001–64.

[36] Miller, R. E., Tadmor, E. B., Phillips, R., Ortiz, M., Jan. 1999. Quasicontinuum simulation of fracture at the atomic scale. Modelling and Simulation in Materials Science and Engineering 6 (5), 607–638.

[37] Murdoch, A. I., Apr. 2010. On Molecular Modelling and Continuum Concepts. Journal of Elasticity 100 (1-2), 33–61.

[38] Noll, W., 1955. Die Herleitung der Grundgleichungen der Thermomechanik der Kontinua aus der statistischen Mechanik. J. Ration. Mech. Anal. 4, 627–646.

[39] Pandurangan, V., Li, H., Ng, T. Y., Aug. 2010. A concurrent multiscale method based on the alternating Schwarz scheme for coupling atomic and continuum scales with first-order compatibility. Computational Mechanics 47 (1), 1–16.

[40] Park, H. S., Karpov, E. G., Klein, P. A., Liu, W. K., Aug. 2005. Three-dimensional bridging scale analysis of dynamic fracture. Journal of Computational Physics 207 (2), 588–609.

[41] Pfaller, S., Possart, G., Steinmann, P., Rahimi, M., Müller-Plathe, F., Böhm, M. C., Nov. 2011. A comparison of staggered solution schemes for coupled particle—continuum systems modeled with the Arlequin method. Computational Mechanics 49 (5), 565–579.

[42] Pfaller, S., Rahimi, M., Possart, G., Steinmann, P., Müller-Plathe, F., Böhm, M. C., Jun. 2013. An Arlequin-based method to couple molecular dynamics and

finite element simulations of amorphous polymers and nanocomposites. Computer Methods in Applied Mechanics and Engineering 260, 109–129.

[43] Plimpton, S., 1995. Fast parallel algorithms for short-range molecular dynamics. Journal of Computational Physics 117 (1), 1–19.

[44] Prudhomme, S., Ben Dhia, H., Bauman, P. T., Elkhodja, N., Oden, J. T., Jul. 2008. Computational analysis of modeling error for the coupling of particle and continuum models by the Arlequin method. Computer Methods in Applied Mechanics and Engineering 197 (41-42), 3399–3409.

[45] Qian, D., Wagner, G. J., Liu, W. K., May 2004. A multiscale projection method for the analysis of carbon nanotubes. Computer Methods in Applied Mechanics and Engineering 193 (17-20), 1603–1632.

[46] Qu, S., Shastry, V., Curtin, W. A., Miller, R. E., Sep. 2005. A finite-temperature dynamic coupled atomistic/discrete dislocation method. Modelling and Simulation in Materials Science and Engineering 13 (7), 1101–1118.

[47] Ramisetti, S. B., Anciaux, G., Molinari, J. F., 2013. Spatial filters for bridging molecular dynamics with finite elements at finite temperatures. Computer Methods in Applied Mechanics and Engineering 253, 28–38.

[48] Saether, E., Yamakov, V., Glaessgen, E. H., Jun. 2009. An embedded statistical method for coupling molecular dynamics and finite element analyses. International Journal for Numerical Methods in Engineering 78 (11), 1292–1319.

[49] Shenoy, V. B., Miller, R. E., Tadmor, E. B., Phillips, R., Ortiz, M., Jan. 1998. Quasicontinuum models of interfacial structure and deformation. Physical Review Letters 80, 742–745.

[50] Smith, E. R., Heyes, D. M., Dini, D., Zaki, T. A., 2012. Control-volume representation of molecular dynamics. Physical Review E 85 (5), 056705.

[51] Su, Z. C., Tan, V. B. C., Tay, T. E., Jun. 2012. Concurrent multiscale modeling of amorphous materials in 3D. International Journal for Numerical Methods in Engineering 92 (13), 1081–1099.

[52] Tadmor, E. B., Ortiz, M., Phillips, R., 1996. Quasicontinuum analysis of defects in solids. Philosophical Magazine A: Physics of Condensed Matter, Structure, Defects and Mechanical Properties 73, 1529–1563.

[53] Templeton, J. A., Jones, R. E., Wagner, G. J., Nov. 2010. Application of a field-based method to spatially varying thermal transport problems in molecular dynamics. Modelling and Simulation in Materials Science and Engineering 18 (8), 085007.

[54] Wagner, G. J., Jones, R. E., Templeton, J. A., Parks, M. L., Jul. 2008. An atomistic-to-continuum coupling method for heat transfer in solids. Computer Methods in Applied Mechanics and Engineering 197 (41-42), 3351–3365.

[55] Wagner, G. J., Liu, W. K., Sep. 2003. Coupling of atomistic and continuum simulations using a bridging scale decomposition. Journal of Computational Physics 190 (1), 249–274.

[56] Xu, M., Gracie, R., Belytschko, T., 2010. A continuum-to-atomistic bridging domain method for composite lattices. International Journal for Numerical Methods in Engineering 81, 1635–1658.

[57] Zhang, S., Khare, R., Lu, Q., Belytschko, T., 2007. A bridging domain and strain computation method for coupled atomistic–continuum modelling of solids. International Journal for Numerical Methods in Engineering 70 (8), 913–933.

[58] Zhang, X., Lu, G., Curtin, W. A., 2013. Multiscale quantum/atomistic coupling using constrained density functional theory. Physical Review B - Condensed Matter and Materials Physics 87 (5).

[59] Zimmerman, J. A., Jones, R. E., Templeton, J. A., Mar. 2010. A material frame approach for evaluating continuum variables in atomistic simulations. Journal of Computational Physics 229 (6), 2364–2389.